ARTICLES
https://doi.org/10.1038/s41589-019-0423-2
nature chemical biology

Dynamics of the context-specific translation arrest by chloramphenicol and linezolid

Junhong Choi[1,2,4,6], James Marks[3,5,6], Jingji Zhang[1], Dong-Hua Chen[1], Jinfan Wang[1], Nora Vázquez-Laslop[3*], Alexander S. Mankin[3*] and Joseph D. Puglisi[1*]

Chloramphenicol (CHL) and linezolid (LZD) are antibiotics that inhibit translation. Both were thought to block peptide-bond formation between all combinations of amino acids. Yet recently, a strong nascent peptide context-dependency of CHL- and LZD-induced translation arrest was discovered. Here we probed the mechanism of action of CHL and LZD by using single-molecule Förster resonance energy transfer spectroscopy to monitor translation arrest induced by antibiotics. The presence of CHL or LZD does not substantially alter dynamics of protein synthesis until the arrest-motif of the nascent peptide is generated. Inhibition of peptide-bond formation compels the fully accommodated A-site transfer RNA to undergo repeated rounds of dissociation and nonproductive rebinding. The glycyl amino-acid moiety on the A-site Gly-tRNA manages to overcome the arrest by CHL. Our results illuminate the mechanism of CHL and LZD action through their interactions with the ribosome, the nascent peptide and the incoming amino acid, perturbing elongation dynamics.

During translation, the ribosome catalyzes peptide-bond formation between chemically and structurally diverse substrates. To accomplish this task, the ribosome precisely positions the peptidyl-tRNA (pept-tRNA) in the P site and aminoacyl-tRNA (aa-tRNA) in the A site[1]. The formation of the new peptide bond results in the transfer of the nascent peptide from the P- to the A-site tRNA, extending the nascent peptide by a single amino acid. On peptidyl transfer, the 50S subunit rotates by 7–10° relative to the 30S subunit[2–6] and tRNAs assume the hybrid state, with their anticodons remaining in the P and A sites in the small subunit, but their acceptor ends moved to the P and E sites in the large subunit (P/E and A/P tRNA states)[4,7]. A subsequent translocation step moves the messenger RNA and tRNA anticodon stem-loops to the E and P sites with the ribosome ratcheting back to the nonrotated state. Various intermediate rotation[8–10] and small-subunit conformational[11] states are sampled during these transitions, although some of them might be too short-lived to be experimentally identified.

Many protein synthesis inhibitors act by sterically disrupting the association and/or positioning of the substrates in the peptidyl-transferase center (PTC) and thus blocking peptide-bond formation[12–15]. Two such small molecules are the antibiotics CHL and LZD (Fig. 1a). CHL is a long-known antibiotic initially isolated from *Streptomyces venezuelae*[16], whereas LZD is a newer synthetic drug and the first representative of the oxazolidinone class of ribosome inhibitors approved for clinical use[17]. Despite their structural differences, both CHL and LZD bind to the same site in the PTC[5,18–21], where they are expected to clash with the A-site aminoacyl moiety on the aa-tRNA. Therefore, CHL and LZD were initially proposed to be nondiscriminatory inhibitors of peptide-bond formation[20,22], by occluding the correct positioning of any aa-tRNA aminoacyl moiety in the PTC active site. However, recent in vivo (Ribo-seq) and in vitro (toeprinting) results showed that neither CHL nor LZD acts as a universal inhibitor of peptide-bond formation[23]. Rather than stopping the ribosome with equal efficiency at every codon, CHL and LZD allow for translation progression through some codons until the ribosomes synthesize nascent peptides with specific features that facilitate translation arrest by the antibiotic. Ribo-seq and toeprinting analyses revealed that CHL and LZD most efficiently exert their inhibitory activity when the ribosome carries a nascent peptide whose penultimate amino acid is an Ala, Ser or Thr[23]. The acceptor substrate (the incoming aa-tRNA) also plays an important role: despite carrying a nascent peptide with a penultimate Ala (or Ser/Thr), a CHL-bound ribosome can still catalyze peptide-bond formation if Gly-tRNA^{Gly} enters the A site[23]. Thus, instead of CHL and LZD being universal inhibitors of translation, the action of these drugs depends strongly on the identities of the ribosomal P- and A-site substrates.

It remains unclear how the combined action of the nascent peptide and CHL or LZD induces translation arrest and which steps of translation leading to peptidyl transfer are affected. It is feasible that the acceptor substrate (aa-tRNA) is rejected at the early stages of its interaction with the ribosome, as has been observed with some other ribosome inhibitors[24], or that tRNA fully accommodates in the A site but subsequent peptide-bond formation is prevented. Furthermore, the mechanism of translation rescue by the A-site Gly-tRNA^{Gly} specific for CHL is unclear, as potentially both the glycine amino acid and the glycine-specific tRNA may contribute to overcoming the antibiotic action. Finally, it is unknown whether CHL and LZD stabilize specific conformational and compositional states of an actively translating ribosome conducive to translation arrest.

To understand the molecular mechanism underlying context-dependent protein synthesis inhibition by CHL and LZD, we combined biochemical and single-molecule Förster resonance energy transfer (smFRET) approaches to monitor CHL or LZD-induced translational arrests. We demonstrate that at the arrest site,

[1]Department of Structural Biology, Stanford University School of Medicine, Stanford, CA, USA. [2]Department of Applied Physics, Stanford University, Stanford, CA, USA. [3]Center for Biomolecular Sciences, University of Illinois, Chicago, IL, USA. [4]Present address: Department of Genome Sciences, University of Washington, Seattle, WA, USA. [5]Present address: National Institute of Arthritis and Musculoskeletal and Skin Diseases, National Institutes of Health, Bethesda, MD, USA. [6]These authors contributed equally: Junhong Choi, James Marks. *e-mail: nvazquez@uic.edu; shura@uic.edu; puglisi@stanford.edu

the presence of CHL allows full accommodation of aa-tRNA body, but prevents the acceptor amino acid from participating in peptide-bond formation with specific donor peptidyl-tRNA substrates. Drug-induced inhibition of the peptidyl-transfer reaction leads to multiple rounds of futile accommodation and dissociation of aa-tRNA without translation progression. We show that the ability of Gly-tRNA^{Gly} to overcome translation stall is determined by the nature of its aminoacyl moiety rather than the tRNA^{Gly} body, highlighting the exceptional properties of glycine as a peptidyl acceptor in the CHL-arrested ribosome.

Results

CHL/LZD context specificity reproduced with model mRNA. Based on the results of our previous Ribo-seq analysis[23] of the effects of CHL and LZD, we designed three model mRNAs encoding peptides with the sequences MFKAFKNIIRTRTL, MFKYFKNIIRTRTL and MFKAFGNIIRTRTL for use in smFRET experiments (see below) (for the further discussion of these model sequences we refer only to the underlined first six amino acids or the codons specifying them; full template sequences are shown in Supplementary Fig. 1). These model mRNA constructs differ minimally in their nucleotide and amino acid sequences but are expected to vary drastically in their ability to promote CHL- and LZD-induced translation arrest at the F_5 codon. The specificity of CHL- and LZD-induced ribosomal arrest was first validated using in vitro toeprinting analysis[23,25] (Fig. 1b). As expected, ribosomes synthesizing the MFKAFK sequence in the presence of either CHL or LZD were arrested with the F_5 codon of the open reading frame (ORF) in the P site and the K_6 codon in the A site, precisely when the nascent peptide contained an Ala residue in the penultimate position (Fig. 1b, lanes 2–4). This result is consistent with the ribosome being unable to catalyze peptide-bond formation between the C-terminal Phe of the MFKAF nascent peptide and the incoming Lys residue in the presence of CHL or LZD. In contrast, synthesis of the MFKYFK peptide, whose fourth residue is a Tyr instead of an Ala, proceeds unimpeded beyond the F_5 codon despite the presence of inhibitory concentrations of CHL or LZD in the reaction (Fig. 1b, lanes 6–8 and Supplementary Fig. 2). Similarly, no CHL-induced translation arrest was observed with the mRNA encoding the MFKAFG peptide (Fig. 1b, lanes 10 and 11). Therefore, ribosomes carrying the MFKAF peptide with a penultimate Ala residue, which typically favors blocking of aa-tRNA incorporation by CHL, successfully catalyze peptidyl transfer to Gly in spite of the presence of this drug. In line with our previous findings[23], LZD is still able to inhibit peptide-bond formation even with Gly as an acceptor (Fig. 1b, lane 12). The results of the cell-free translation experiments with the model templates are fully consistent with and recapitulate the context-specific effects of CHL and LZD observed in vivo[23] and justify the use of these designed ORFs for studying the mechanistic basis of action of these antibiotics in vitro.

Monitoring CHL/LZD-induced translation arrest in real time. We next characterized CHL- and LZD-induced translation arrest using a smFRET-based translation assay[26–28] (Fig. 2a). To monitor multiple rounds of translation elongation that report CHL and LZD effects, we labeled *Escherichia coli* ribosomal small subunits at helix 44 with Cy3B (Cy3B-30S) and labeled large subunits at helix 101 with the quencher BHQ-2 (BHQ-50S)[27,29]. The one-color FRET signal between the dyes allows the monitoring of ribosomal conformation changes during translation (Fig. 2a, green trace). Before aa-tRNA binding, the ribosome assumes a nonrotated state, characterized by substantially quenched Cy3B fluorescence state because of its proximity to BHQ-2 on the large ribosomal subunit. On the aa-tRNA accommodation, the peptidyl-transfer reaction induces a transition to the rotated state, detected as a higher Cy3B intensity due to the increased distance between Cy3B and BHQ-2.

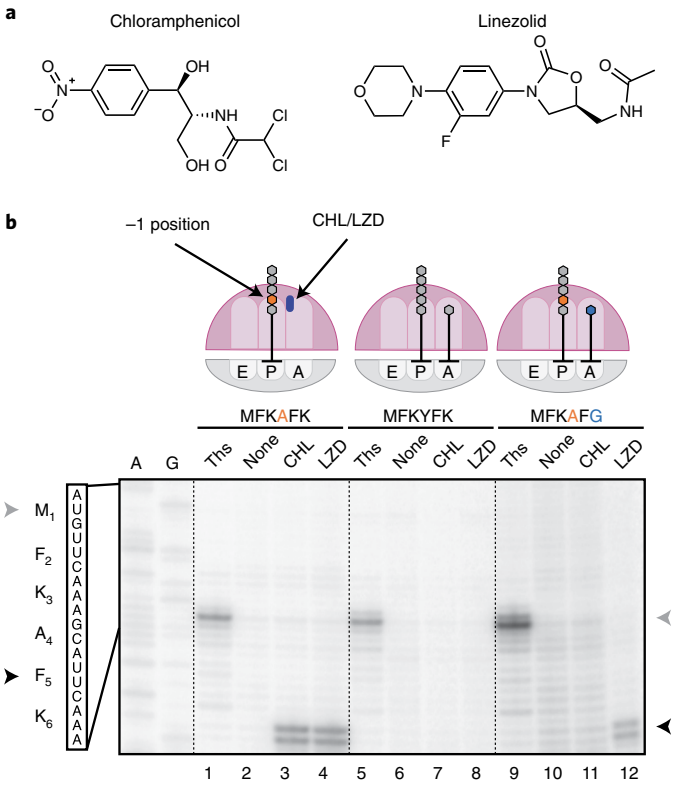

Fig. 1 | Context-specific inhibition of translation by CHL and LZD. **a**, Chemical structures of antibiotics CHL and LZD. **b**, In vitro toeprinting analysis of CHL- or LZD-induced translational arrest on three different mRNA constructs (complete sequences of the templates are shown in Supplementary Fig. 1, independently repeated at least twice with similar results). The toeprint bands produced by CHL- or LZD-arrested ribosomes at the F_5 codon of the mRNAs are indicated by black arrowheads. Gray arrowheads show the toeprint bands produced by ribosomes stalled at the start codons due to the presence of thiostrepton (Ths). Sequencing lanes A and G for the MFKAFK template are shown.

Subsequently, translocation of the ribosome to the next codon resets the nonrotated state with the deacylated tRNA rapidly departing from the E site[30], completing one cycle of translation elongation. To increase further the accuracy of the assignment of translation cycles based on monitoring the intersubunit rotation, we used the binding of fluorescently labeled tRNA^{Phe} labeled with Cy5 (at the naturally modified acp^{3}U47 residue[31], see Methods) at the F_2 and F_5 codons[28] (Fig. 2a, red trace). The tRNA signal appears when aa-tRNA binds to the A site of the ribosome and persists after its translocation to the P site until the subsequent cycle of elongation places labeled tRNA in the E site for dissociation.

Fluorescence intensity states corresponding to the nonrotated and rotated state for translating the first five codons were assigned as follows: a decrease in the Cy3B fluorescence intensity followed by a concurrent increase of both Cy3B and Cy5 intensities were assigned as a translation initiation event (binding of BHQ-50S to the surface-tethered mRNA–Cy3B-30S pre-initiation complex) and transition from nonrotated to rotated state for decoding of the first Phe (F_2) codon and first peptide-bond formation, respectively (Fig. 2a,b). Observed nonrotated and rotated intensity levels observed during this translation of the first F_2 codon were used to assign subsequent Cy3B fluorescence intensity changes between the nonrotated and rotated states for the first five codons (F_2-K_3-A_4-F_5-K_6) following the start codon M_1 in the MFKAFK mRNA construct. Concurrent decreases of the Cy3B and Cy5 intensities were

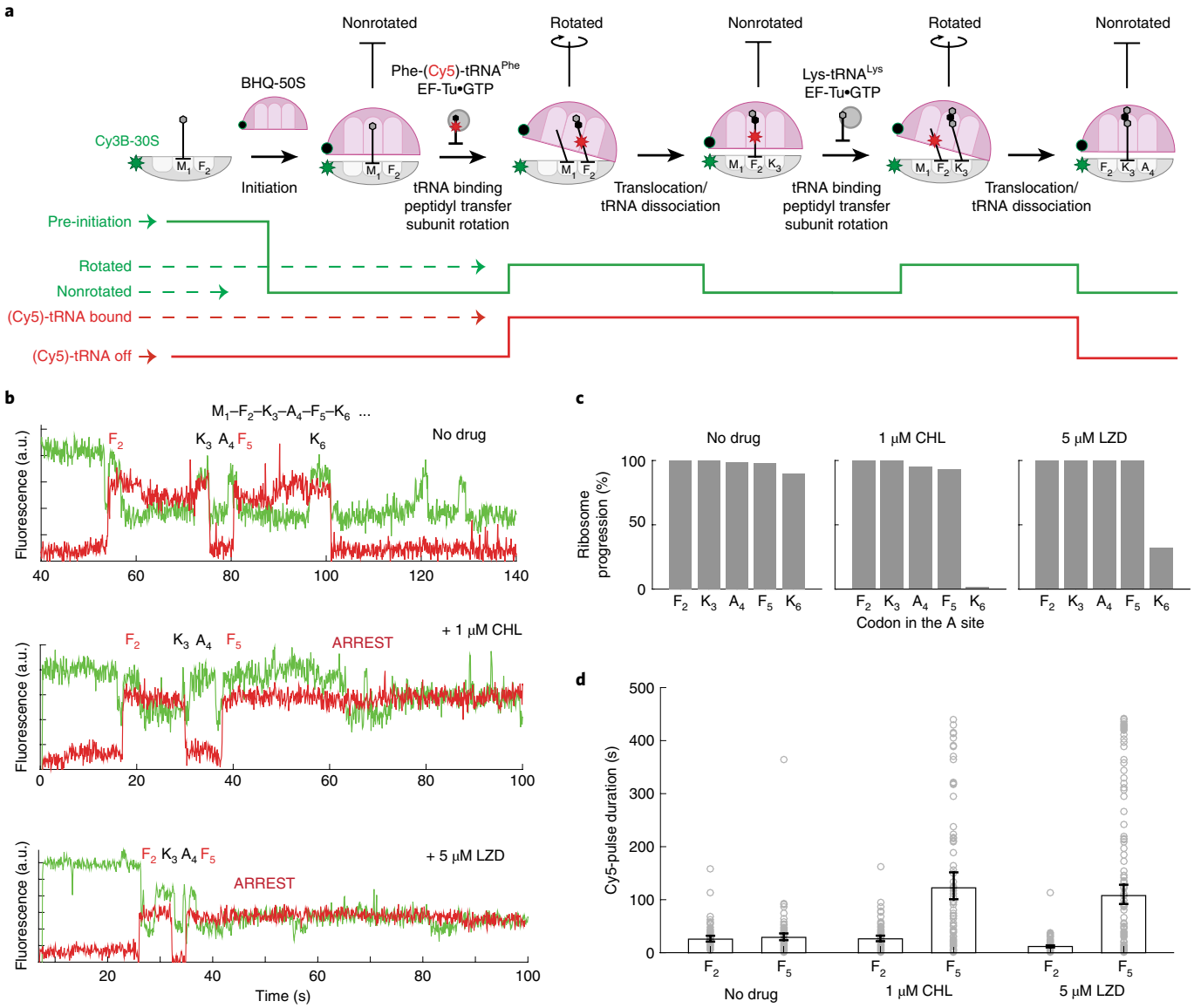

Fig. 2 | Monitoring the drug-induced translation arrest using smFRET-based assay. a, Top, diagram of smFRET-based assay to monitor ribosome structural changes coupled to translation elongation progression. Using Cy3B–BHQ-2 dye-quencher pair, nonrotated and rotated ribosome conformations are tracked. Binding of labeled specific tRNA (Phe-(Cy5)-tRNA^{Phe}) is used to enhance fidelity of state transitions. Bottom, diagram of expected fluorescence intensities matching the structural states depicted immediately above. **b**, Representative traces for experiments without any antibiotics (similar results observed for $n = 87$, 100 and 139 for conditions 'no drug', '1 μM CHL' and '5 μM LZD', respectively). **c**, Processivity of translation over the first six codons within the mRNA ORF at different conditions, measured as percentage of ribosomes that translated a particular codon over the entire population. **d**, Measurement of Cy5 pulse durations from Phe-(Cy5)-tRNA^{Phe} binding events at Phe codon 2 (F_2) and Phe codon 5 (F_5) for different conditions. Error bars represent a 95% confidence interval from fitting the single-exponential distribution. Sample sizes for each condition are identical in **b**–**d**.

used as a criterion for assigning the complete translation of two Lys codons (K_3 and K_6), placed following two Phe codons (F_2 and F_5). We have used this criterion to avoid the misassignment of Cy3B signal fluctuation as a rapid translation event. In previous studies, we have compared kinetic measurements from this smFRET setup with the ensemble kinetic measurements, and have observed a close agreement in detecting the effect of mRNA modifications to translation decoding kinetics between the two measurement schemes[32,33].

By monitoring real-time translation elongation in the presence of 1 μM CHL or 5 μM LZD, we observed a strong arrest of translation at codon F_5 of the MFKAFK template, when Ala is present at the penultimate position of the nascent peptide (Fig. 2b, middle and bottom traces). An arrest does not occur in the absence of the inhibitors (Fig. 2b, upper traces). In the presence of CHL or LZD, on translocation to the arrest site (F_5 codon in the P site), the ribosome does not transition to a stable rotated state, indicating that the aa-tRNA binding and/or peptidyl transfer is inhibited. CHL inhibited translation more efficiently and at lower concentrations than LZD: at 1 μM CHL, 98 ± 2% of the translating ribosomes were halted at the arrest site, while the effect of LZD was only evident at 5 μM LZD (68 ± 4% arrested ribosomes) (Fig. 2c). The measured lifetime of ribosome occupancy by Phe-(Cy5)-tRNA^{Phe} shows that the presence of CHL or LZD had little effect on the kinetics of tRNA transitioning through all three tRNA binding sites at the F_2 codon of the MFKAFK template (Fig. 2a,d). In contrast, the second Cy5 pulse lifetime corresponding to the F_5 codon was substantially prolonged in the presence of the drugs. The measured Cy5 pulse lifetime of ~120 s at the F_5 arrest codon (compared to the lifetime of ~25 s

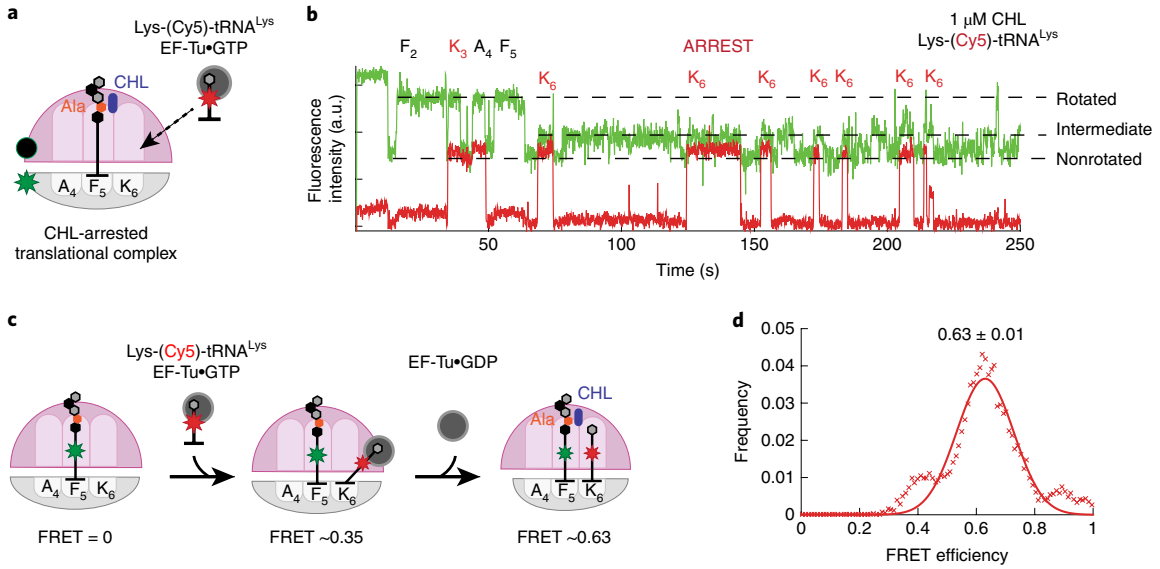

Fig. 3 | Monitoring accommodation of A-site tRNA during CHL-induced translational arrest. a,**b**, Monitoring the binding of Lys-(Cy5)-tRNA^{Lys} to the ribosome translating the MFKAFK template in the presence of CHL; schematics of the experiment (**a**) and a representative trace (**b**). The multiple appearance of the intermediate FRET state coincides with the binding of Lys-(Cy5)-tRNA^{Lys}. On average, Cy5 pulses were observed 3.5 times per translating ribosomes at codon 6 (n = 104 number of ribosomes) **c**, Schematics of tRNA–tRNA FRET experiment on CHL-arrested ribosome. FRET efficiencies report on the accommodation states of the A-site tRNA (schematics and FRET efficiencies adapted from Polikanov et al.[24]). **d**, smFRET efficiencies (x axis) between the P-site tRNA (fMet-Phe-Lys-Ala-Phe-(Cy3)-tRNA^{Phe}) on codon 5 (F_5) and incoming A-site tRNAs (Lys-(Cy5)-tRNA^{Lys}) on codon 6 (K_6), and fitted normal distribution (red line) (n = 121 molecules or 186 individual FRET events).

at the F_2 nonarrest codon) is comparable to the Cy5 dye lifetime before photobleaching[34], suggesting that the actual duration of the translation arrest in our system could be even longer. Nonetheless, this result independently confirms the trapping of the ribosome by antibiotics after the F_5 codon of the MFKAFK mRNA is placed in the P site.

When the penultimate alanine (A_4) residue is changed to tyrosine (Y_4) in the MFKYFK construct, neither CHL nor LZD prevents ribosomes from translating the MFKYFK sequence (Supplementary Fig. 3a,b), confirming that our single-molecule assay recapitulates the specificity of the drug-dependent arrest. Furthermore, the presence of the drugs did not alter the kinetics of translation at any of the codons of the MFKYFK sequence (Supplementary Fig. 3c), which indicates that CHL or LZD prevents the incorporation of the incoming amino acid predominantly when the ribosome carries nascent peptides with specific sequences. The single-molecule data thus confirm and agree with previous biochemical results on the context-specific stalling in the presence of CHL or LZD. Since CHL was more active in our assays, most of the subsequent experiments were carried out with this drug.

Futile sampling of aa-tRNA to the CHL-arrested ribosome. To elucidate the state of the ribosome during the antibiotic-induced arrest, we monitored the binding of the A-site tRNA. Here, we used Lys-(Cy5)-tRNA^{Lys} instead of Phe-(Cy5)-tRNA^{Phe} to cross-correlate elongation cycles deduced from the intersubunit FRET. In the presence of 1 μM CHL, the ribosome efficiently translated the first codons of the MFKAFK template (Fig. 3a,b). However, when the F_5 codon translocated to the P site of the CHL-bound ribosome, subsequent rounds of translocation were inhibited. Instead, we observed multiple bindings of Lys-(Cy5)-tRNA^{Lys} to the ribosome directed by the K_6 codon positioned in the A site. These tRNA sampling events were uncoupled from the ribosome transition from a nonrotated state to the fully rotated state but corresponded with an intermediate increase in Cy3B fluorescence intensity (referred to as the intermediate FRET state) (Fig. 3b). About 30% of the time, sampling of the intermediate FRET state was observed without the appearance of the Cy5 signal (for example, at 75–125 s in Fig. 3b), which we attributed to binding of an unlabeled cognate Lys-tRNA^{Lys} (present either in the preparation of Lys-(Cy5)-tRNA^{Lys} and/or the bulk aminoacyl-tRNA despite using lysine-depleted amino acid mixture); alternatively this could be caused by binding of an unlabeled near-cognate tRNA after the miscoding event.

We thus observed two unexpected features of the CHL-arrested translational complex: first, repeated cycles of A-site tRNA binding and dissociation occurring at the stall site and second, the transition of the ribosome to a state characterized by the intermediate FRET value that may be related to the cycles of tRNA binding.

aa-tRNA body accommodates into the CHL-stalled ribosome. To investigate the state of tRNAs during sampling of the CHL-arrested translational complex, we monitored smFRET between P- and A-site tRNAs, which reports their relative placement on the ribosome[31,35]. Before the accommodation and positioning of the acceptor aminoacyl residue in the PTC active site, aa-tRNA is delivered to the ribosome in the form of the EF-Tu·GTP·aa-tRNA ternary complex. The ternary complex on the ribosome undergoes conformational transitions that result in different tRNA–tRNA FRET values as the ternary complex progresses from initial interaction with the ribosome to codon recognition, GTPase activation and subsequent accommodation of the aa-tRNA body within the A site[31,36,37]. To follow the tRNA accommodation during the drug-induced arrest, the unlabeled ribosomes were stalled by CHL at the F_5 codon of the MFKAFK mRNA with fMet-Phe-Lys-Ala-Phe-(Cy3)-tRNA^{Phe} in the P site and the binding of Lys-(Cy5)-tRNA^{Lys} encoded by the K_6 codon was monitored following tRNA–tRNA FRET (Fig. 3c). The mean FRET efficiency of tRNA binding events on the arrested ribosome was 0.63 ± 0.01 (Fig. 3d). The high FRET efficiency between two adjacent tRNA suggests that, despite inhibiting the pentapeptidyl transfer to the Lys-tRNA, PTC-bound CHL allows for the full

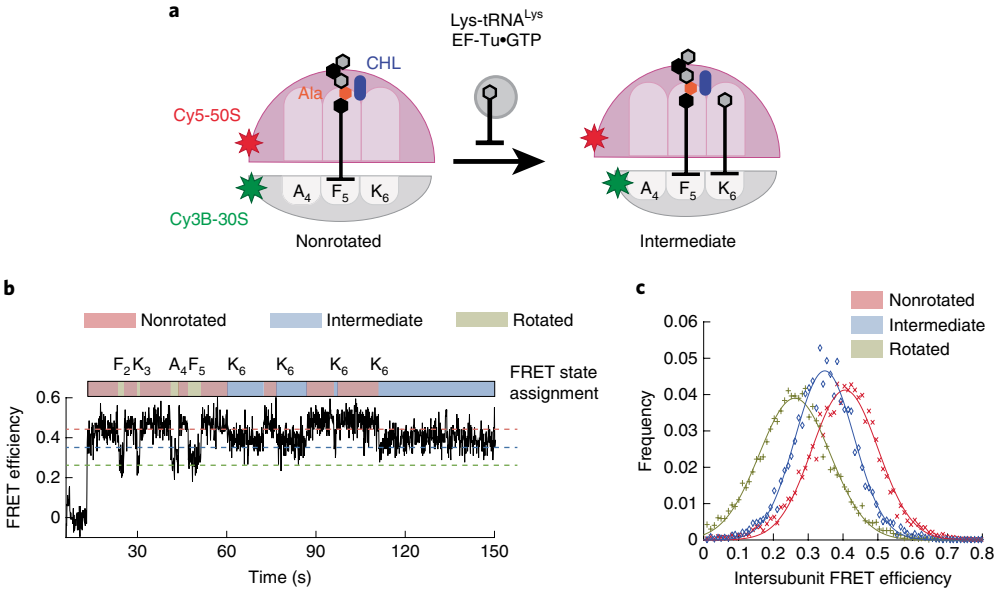

Fig. 4 | Measuring FRET efficiency for the intermediate FRET state during CHL-induced translational arrest. a, Schematic diagram of smFRET assay using Cy3B–Cy5 pair to measure FRET efficiencies of nonrotated, rotated and intermediate FRET states of the ribosome during translation in the presence of CHL. **b**, Representative FRET trace and state assignments for the ribosome translating MFKAFK mRNA in the presence of 1 μM CHL (similar results observed for $n = 94$). **c**, FRET efficiency histogram for each state (plus, x and diamond) and fitted normal distributions (line).

accommodation of the body of the incoming aa-tRNA in the A site during the sampling events. This resembles the effects of some other inhibitors of peptide-bond formation (for example, hygromycin A or A201A) that also block aminoacyl-tRNA entry but apparently act at earlier steps in the tRNA selection pathway[23].

A distinct FRET state is observed during aa-tRNA sampling. Being intrigued by a full, but nonproductive, accommodation of the A-site tRNA, to the drug-stalled ribosome, we wanted to characterize in more detail the ribosome intermediate FRET state that we initially observed using the Cy3B–BHQ intersubunit FRET pair (Fig. 2b). To solidify and expand those observations, we followed the ribosomal conformation using the Cy3B–Cy5 donor–acceptor FRET pair whose anticorrelated signal is less ambiguous than that of Cy3B–BHQ-2 FRET signal[38]. Translation assays were carried out in the presence of unlabeled tRNAs with Cy5 on the large subunit (Cy5–50S) replacing BHQ-2 (Fig. 4a). During translation of the first five codons of the MFKAFK mRNA in the presence of CHL, we observed transitions between high FRET (nonrotated) and low FRET (rotated) states, characterized by average FRET efficiency values of ~0.41 and ~0.26, respectively (Fig. 4b,c, red and green lines), in agreement with previously reported results[38]. However, ribosomes that reached the arrest site (F_5) do not acquire the fully rotated state. Instead, we observed repeated rounds of sampling of a state characterized by an average FRET value of ~0.35 (Fig. 4b,c, blue line) before the Cy3B or Cy5 photobleaching. These data suggest that the nonproductive accommodation of the aa-tRNA in the A site promotes the CHL-arrested ribosome to adapt the state characterized by the intermediate FRET value. Based on the FRET efficiency changes, it is expected that the distance between two labels (Cy3B on 30S subunit helix 44 and Cy5 on helix 101 of 50S subunit) increases by ~3 Å on transitioning from the nonrotated to the CHL-dependent intermediate FRET state: less than half of the distance change (8 Å) from the nonrotated to fully rotated state measured in the same experiment. This state has likely resulted from a conformational change of the 30S subunit known as domain closure[36,39,40] (Supplementary Fig. 4), accompanying the full accommodation of the aminoacyl-tRNA in the A site (see Discussion).

Incoming glycyl-tRNA relieves CHL-induced translation arrest. The presence of CHL (or LZD) prevents peptide-bond formation with the incoming aminoacyl residue when Ala is the penultimate amino acid of the nascent chain, even though CHL (and likely LZD) does not prevent the accommodation of aa-tRNA body in the A site. The CHL-mediated translation block can be circumvented if Gly-tRNA^{Gly} serves as the acceptor substrate[22] (Fig. 1b, compare lanes 3 and 11). In agreement with those findings, approximately 75% of the ribosomes translated past the arrest site of the MFKAFG mRNA construct in the presence of CHL in the smFRET assay (Supplementary Fig. 3a). These data suggest that either the nature of the tRNA itself or of the glycyl moiety is responsible for Gly-tRNA^{Gly} rescue of the drug-mediated arrest. Therefore, we next sought to understand which feature of the A-site Gly-tRNA^{Gly} contributes to the rescue of the drug-stalled ribosome.

To distinguish the contribution of the tRNA^{Gly} body or the aminoacyl residue for circumventing the CHL-induced arrest, we prepared Gly-(Cy5)-tRNA^{Lys} by mischarging Cy5-labeled tRNA^{Lys} with glycine using the flexizyme reaction[41,42] and then employed this substrate in the smFRET translation assay. Here, the Cy3B–BHQ-2 labeled ribosomes, and Gly-(Cy5)-tRNA^{Lys} were used to translate MFKAFK mRNA constructs in the presence or absence of CHL (Fig. 5a). Without CHL, the synthesized Gly-(Cy5)-tRNA^{Lys} successfully participated in the translation of Lys codons, with 87% of ribosomes able to synthesize the MFGAFG peptide sequence (Fig. 5b,c). Even in the presence of 1 μM CHL, 86% of ribosomes translated past the arrest site using Gly-(Cy5)-tRNA^{Lys}, in stark contrast to the only 2% of ribosomes that were able to incorporate lysine (K_6) into the MFKAFK peptide when Lys-(Cy5)-tRNA^{Lys} was used (Fig. 5b,c). Contrary to what was observed with Lys-(Cy5)-tRNA^{Lys} (Fig. 3b), we did not detect rounds of nonproductive binding of Gly-(Cy5)-tRNA^{Lys} to the CHL-bound ribosome. Thus, replacing the aminoacyl moiety of the Lys-tRNA^{Lys} with Gly was sufficient for the bypass of the CHL-induced block of peptide-bond formation.

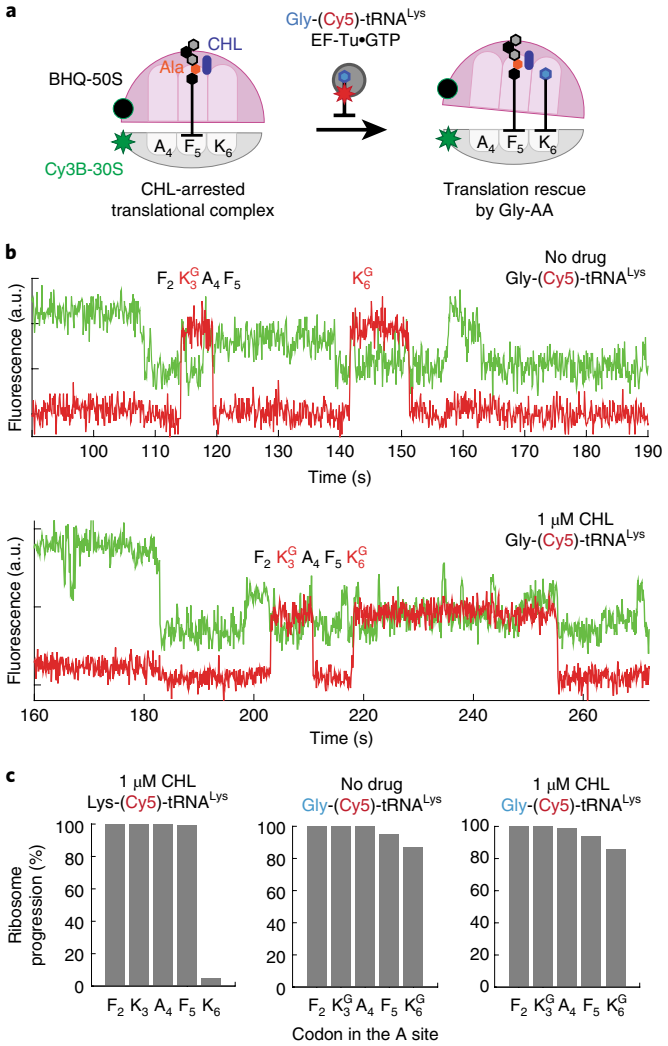

Fig. 5 | The glycyl residue of the A-site tRNA rescues CHL-arrested ribosomes. a, Schematic diagram of experiments using Cy5-labeled tRNA^{Lys} mischarged with Gly (Gly-(Cy5)-tRNA^{Lys}). **b**, Representative fluorescence traces of translation of the MFKAFK mRNA in the reaction containing the mischarged Gly-(Cy5)-tRNA^{Lys} in the absence (top) or presence (bottom) of CHL (similar results observed for $n = 134$ and 120 for top and bottom plots, respectively). **c**, Ribosome survival plots showing that the presence of Gly-tRNA^{Lys} promotes bypassing of the CHL-induced translation arrest at the F_5 codon of the MFKAFK template ($n = 94$, 134 and 120 from left to right).

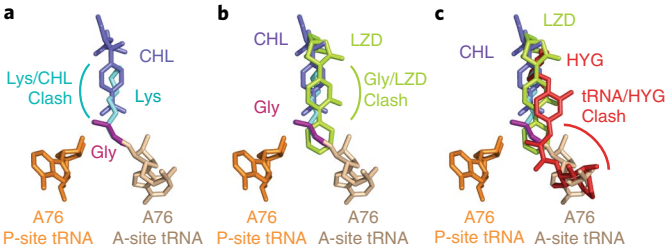

Fig. 6 | Modeling of relative placement of antibiotics and tRNA substrates in the PTC active site. a, Overlay of the bound CHL molecule and the predicted position of the lysine amino acid (Lys) on the A-site tRNA (A76 of both A-site and P-site tRNA shown; adapted based on PDB 1VY4 (ref. [45]) and amino-acid residues modeled). Lys is likely to clash with CHL (PDB 4V7T, ref. [43]), while the glycine (Gly) moiety can be properly accommodated without a direct steric clash. **b**, Overlay of the LZD (PDB 3CPW, ref. [44]) with CHL and tRNAs bound to the A site and P site of the ribosome. LZD is likely to clash with Gly on the A-site tRNA. **c**, Overlay of hygromycin A (HYG) with CHL and LZD (PDB 5DOY, ref. [24]). HYG is likely to clash directly with the A76 of A-site tRNA.

This agrees well with our observation of the full accommodation of the A-site tRNA^{Lys} during the CHL-induced translational arrest (Fig. 3d): when the body of tRNA is fully accommodated, the bulky lysine residue is likely displaced by CHL from the PTC active site, whereas glycine, that lacks the side chain, achieves proper positioning to participate in the peptide-bond formation reaction. Thus, our data demonstrate that not only penultimate amino acid of the nascent chain, but also the identity of the A-site amino acid critically contributes to defining the sites of CHL-induced translation arrest.

To understand how Gly acceptor amino acid can rescue translation, we modeled the structure of the drug-bound PTC based on the available structures[24,43–45]. Because of the lack of side chain, the clash of Gly with the CHL molecule in the A site is greatly diminished (Fig. 6a), thereby possibly allowing the Gly acceptor to reach the configuration required to participate in peptide-bond formation. The avoidance of the clash is less likely when LZD is bound in the PTC (Fig. 6b), possibly explaining why Gly acceptor amino acid rescues CHL-, but not LZD-induced arrest.

The context specificity of action of CHL and LZD has not been demonstrated for several other inhibitors that also bind in the PTC A site. One such example is hygromycin A, an antibiotic whose binding site overlaps with the sites of action of CHL and LZD[23] (Fig. 6c). Hygromycin A, that clashes not only with the aminoacyl moiety, but also with the 3′ terminal adenosine of the aa-tRNA, can efficiently arrest the ribosomes at start codons of the genes by inhibiting the tRNA accommodation in the A site[23], in contrast to CHL or LZD, both of which fail to inhibit the first peptide-bond formation even when present at high concentrations[23,25].

Discussion

The dynamic single-molecule fluorescence results presented here complement and extend the biochemical data and provide mechanistic insights into the drastic effect of CHL and LZD on elongation pathways within a given nascent-peptide chain context. As previously shown[23], if a nascent peptide contains any amino acid but Ala (or Ser/Thr) in the penultimate position, then the following round of elongation proceeds relatively unimpeded despite the presence of the inhibitor. However, when the penultimate amino acid of the nascent peptide is an Ala (or Ser/Thr), translation is arrested.

We observed that at the site of the CHL-induced arrest, the ribosome can bind, and accommodate the body of the A-site aa-tRNA, but peptide-bond formation does not take place possibly due to the displacement of the incoming amino acid and/or the nascent-peptide chain. Cognate codon-anticodon interaction in the decoding center, that must take place for the aa-tRNA accommodation, results in the conformational change of the 30S subunit known as domain closure[36,39,40]. Such structural rearrangement of the small subunit relocates the placement of the tip of the small subunit helix 44 where our fluorophore was attached, relative to the large subunit. Therefore, the conformational change of the small subunit, induced by aa-tRNA accommodation, could explain the intermediate intersubunit FRET state observed in our smFRET experiments during unproductive rounds of binding of aa-tRNA at the site of the drug-induced arrest. The same intermediate intersubunit FRET signal has been interpreted as a partially rotated state of the ribosome in our previous report[30], caused by the presence of the E-site tRNA. However, in light of our new data, we favor the view that intermediate FRET state reports the 30S domain closure after the tRNA accommodation event and is the on-pathway rearrangement that,

in the absence of antibiotic, would be followed by placement of the acceptor amino acid in the PTC A site, peptide-bond formation and intersubunit rotation. Normally this would be a transient state not observed by our smFRET assays, but in the presence of CHL, LZD or E-site tRNA, the duration of this domain-closed state is extended and detected. Further, in the case of CHL or LZD-induced translation arrest, the inability of the drug-bound ribosome to catalyze the formation of the peptide bond prevents subsequent transition and instead results in tRNA dissociation and subsequent rounds of aa-tRNA sampling and 30S domain closure.

We can envision two compatible mechanisms that could account for the context specificity of CHL and LZD action defined by the nature of the penultimate amino acid of the nascent chain. First, the penultimate amino acid residue of a stalling nascent peptide may increase the affinity of CHL and LZD to the ribosome, facilitating their competition with the accommodating aa-tRNA. The bound antibiotic would not prevent the accommodation of the tRNA body but would preclude the proper placement of the acceptor substrate in the PTC active site, leading to translation arrest at codons that follow those specifying Ala, Ser or Thr. Second, CHL and LZD may also alter the positioning of the nascent peptide when its penultimate residue is Ala, Ser or Thr, displacing the ester group of the donor substrate from its optimal placement for the nucleophilic attack of the acceptor amino acid α-amino group. The conformational manipulation of both the donor and acceptor peptidyl-transfer substrates may be similar to inhibition mechanisms observed in the poly-proline track, where it has been assumed that not only the restricted acceptor substrate conformation but also maneuvering of the nascent peptide placement are required for translational arrest[46]. Determining whether either or both mechanisms above underlie antibiotic-induced translational arrest requires additional investigations.

Both CHL and LZD have been demonstrated to induce miscoding[47], and our work suggests a possible mechanism of how the context specificity of CHL and LZD could induce that effect. Unsuccessful samplings of the cognate tRNA without peptide-bond formation open an opportunity for a near-cognate tRNA to deliver an amino acid (for example, glycine) with a diminished clash with the antibiotic resulting in its incorporation and continued translation. As previously mentioned, this context specificity of action has not been demonstrated for several other inhibitors, such as hygromycin A, that also bind in the PTC A site and efficiently arrest the first peptide-bond formation at the start codon[23], suggesting a peptide-context independent mechanism of action. Such different context dependencies among antibiotics that inhibit peptidyl-transfer reaction may suggest that combinations of structural, genetic and kinetic assays are needed to determine the precise mechanism of action for a given drug.

Online content

Any methods, additional references, Nature Research reporting summaries, source data, extended data, supplementary information, acknowledgements, peer review information; details of author contributions and competing interests; and statements of data and code availability are available at https://doi.org/10.1038/s41589-019-0423-2.

Received: 7 June 2019; Accepted: 30 October 2019;
Published online: 16 December 2019

References

1. Rodnina, M. V. & Wintermeyer, W. Peptide bond formation on the ribosome: structure and mechanism. *Curr. Opin. Struct. Biol.* **13**, 334–340 (2003).
2. Frank, J. & Agrawal, R. K. A ratchet-like inter-subunit reorganization of the ribosome during translocation. *Nature* **406**, 318–322 (2000).
3. Valle, M. et al. Locking and unlocking of ribosomal motions. *Cell* **114**, 123–134 (2003).
4. Agirrezabala, X. et al. Visualization of the hybrid state of tRNA binding promoted by spontaneous ratcheting of the ribosome. *Mol. Cell* **32**, 190–197 (2008).
5. Dunkle, J. A. et al. Structures of the bacterial ribosome in classical and hybrid states of tRNA binding. *Science* **332**, 981–984 (2011).
6. Ermolenko, D. N. et al. Observation of intersubunit movement of the ribosome in solution using FRET. *J. Mol. Biol.* **370**, 530–540 (2007).
7. Moazed, D. & Noller, H. F. Intermediate states in the movement of transfer RNA in the ribosome. *Nature* **342**, 142–148 (1989).
8. Munro, J. B., Altman, R. B., O'Connor, N. & Blanchard, S. C. Identification of two distinct hybrid state intermediates on the ribosome. *Mol. Cell* **25**, 505–517 (2007).
9. Bock, L. V. et al. Energy barriers and driving forces in tRNA translocation through the ribosome. *Nat. Struct. Mol. Biol.* **20**, 1390–1396 (2013).
10. Jamiolkowski, R. M., Chen, C., Cooperman, B. S. & Goldman, Y. E. tRNA fluctuations observed on stalled ribosomes are suppressed during ongoing protein synthesis. *Biophys. J.* **113**, 2326–2335 (2017).
11. Voorhees, R. M. & Ramakrishnan, V. Structural basis of the translational elongation cycle. *Annu. Rev. Biochem.* **82**, 203–236 (2013).
12. Polacek, N. & Mankin, A. S. The ribosomal peptidyl transferase center: structure, function, evolution, inhibition. *Crit. Rev. Biochem. Mol. Biol.* **40**, 285–311 (2005).
13. Wilson, D. N. The A-Z of bacterial translation inhibitors. *Crit. Rev. Biochem. Mol. Biol.* **44**, 393–433 (2009).
14. Lin, J., Zhou, D., Steitz, T. A., Polikanov, Y. S. & Gagnon, M. G. Ribosome-targeting antibiotics: modes of action, mechanisms of resistance, and implications for drug design. *Annu. Rev. Biochem.* **87**, 451–478 (2018).
15. Arenz, S. & Wilson, D. N. Bacterial protein synthesis as a target for antibiotic inhibition. *Cold Spring Harb. Perspect. Med.* **6**, a025361 (2016).
16. Ehrlich, J., Gottlieb, D., Burkholder, P. R., Andierson, L. E. & Pridham, T. G. *Streptomyces venezuelae*, n. sp., the source of chloromycetin. *J. Bacteriol.* **56**, 467–477 (1948).
17. Brickner, S. J., Barbachyn, M. R., Hutchinson, D. K. & Manninen, P. R. Linezolid (ZYVOX), the first member of a completely new class of antibacterial agents for treatment of serious Gram-positive infections. *J. Med. Chem.* **51**, 1981–1990 (2008).
18. Schlunzen, F. et al. Structural basis for the interaction of antibiotics with the peptidyl transferase center in eubacteria. *Nature* **413**, 814–821 (2001).
19. Leach, K. L. et al. The site of action of oxazolidinone antibiotics in living bacteria and in human mitochondria. *Mol. Cell* **26**, 393–402 (2007).
20. Wilson, D. N. et al. The oxazolidinone antibiotics perturb the ribosomal peptidyl-transferase center and effect tRNA positioning. *Proc. Natl Acad. Sci. USA* **105**, 13339–13344 (2008).
21. Bulkley, D., Innis, C. A., Blaha, G. & Steitz, T. A. Revisiting the structures of several antibiotics bound to the bacterial ribosome. *Proc. Natl Acad. Sci. USA* **107**, 17158–17163 (2010).
22. Pestka, S. in *Antibitoics III: Mechanism of Action of Antimicrobial and Antitumor Agents* (eds Corcoran, J. W. & Hahn, F. E.) 370–395 (Springer-Verlag, 1975).
23. Marks, J. et al. Context-specific inhibition of translation by ribosomal antibiotics targeting the peptidyl transferase center. *Proc. Natl Acad. Sci. USA* **113**, 12150–12155 (2016).
24. Polikanov, Y. S. et al. Distinct tRNA accommodation intermediates observed on the ribosome with the antibiotics hygromycin A and A201A. *Mol. Cell* **58**, 832–844 (2015).
25. Orelle, C. et al. Tools for characterizing bacterial protein synthesis inhibitors. *Antimicrob. Agents Chemother.* **57**, 5994–6004 (2013).
26. Aitken, C. E. & Puglisi, J. D. Following the intersubunit conformation of the ribosome during translation in real time. *Nat. Struct. Mol. Biol.* **17**, 793–800 (2010).
27. Dorywalska, M. et al. Site-specific labeling of the ribosome for single-molecule spectroscopy. *Nucleic Acids Res.* **33**, 182–189 (2005).
28. Uemura, S. et al. Real-time tRNA transit on single translating ribosomes at codon resolution. *Nature* **464**, 1012–1017 (2010).
29. Chen, J., Tsai, A., Petrov, A. & Puglisi, J. D. Nonfluorescent quenchers to correlate single-molecule conformational and compositional dynamics. *J. Am. Chem. Soc.* **134**, 5734–5737 (2012).
30. Choi, J. & Puglisi, J. D. Three tRNAs on the ribosome slow translation elongation. *Proc. Natl Acad. Sci. USA* **114**, 13691–13696 (2017).
31. Blanchard, S. C., R. L., Kim, H. D., Chu, S. & Puglisi, J. D. tRNA selection and kinetic proofreading in translation. *Nat. Struct. Mol. Biol.* **11**, 1008–1014 (2004).
32. Choi, J. et al. N6-methyladenosine in mRNA disrupts tRNA selection and translation-elongation dynamics. *Nat. Struct. Mol. Biol.* **23**, 110–115 (2016).
33. Choi, J. et al. 2′-O-methylation in mRNA disrupts tRNA decoding during translation elongation. *Nat. Struct. Mol. Biol.* **25**, 208–216 (2018).
34. Chen, J. et al. High-throughput platform for real-time monitoring of biological processes by multicolor single-molecule fluorescence. *Proc. Natl Acad. Sci. USA* **111**, 664–669 (2014).

35. Wasserman, M. R., Alejo, J. L., Altman, R. B. & Blanchard, S. C. Multiperspective smFRET reveals rate-determining late intermediates of ribosomal translocation. *Nat. Struct. Mol. Biol.* **23**, 333–341 (2016).
36. Loveland, A. B., Demo, G., Grigorieff, N. & Korostelev, A. A. Ensemble cryo-EM elucidates the mechanism of translation fidelity. *Nature* **546**, 113–117 (2017).
37. Alejo, J. L. & Blanchard, S. C. Miscoding-induced stalling of substrate translocation on the bacterial ribosome. *Proc. Natl Acad. Sci. USA.* **114**, E8603–E8610 (2017).
38. Marshall, R. A., Aitken, C. E. & Puglisi, J. D. GTP hydrolysis by IF2 guides progression of the ribosome into elongation. *Mol. Cell* **35**, 37–47 (2009).
39. Fislage, M. et al. Cryo-EM shows stages of initial codon selection on the ribosome by aa-tRNA in ternary complex with GTP and the GTPase-deficient EF-TuH84A. *Nucleic Acids Res.* **46**, 5861–5874 (2018).
40. Brilot, A. F., Korostelev, A. A., Ermolenko, D. N. & Grigorieff, N. Structure of the ribosome with elongation factor G trapped in the pretranslocation state. *Proc. Natl Acad. Sci. USA* **110**, 20994–20999 (2013).
41. Murakami, H., Ohta, A., Ashigai, H. & Suga, H. A highly flexible tRNA acylation method for non-natural polypeptide synthesis. *Nat. Methods* **3**, 357–359 (2006).
42. Goto, Y. & Suga, H. Translation initiation with initiator tRNA charged with exotic peptides. *J. Am. Chem. Soc.* **131**, 5040–5041 (2009).
43. Dunkle, J. A., Xiong, L., Mankin, A. S. & Cate, J. H. D. Structures of the *Escherichia coli* ribosome with antibiotics bound near the peptidyl transferase center explain spectra of drug action. *Proc. Natl Acad. Sci. USA* **107**, 17152–17157 (2010).
44. Ippolito, J. A. et al. Crystal structure of the oxazolidinone antibiotic linezolid bound to the 50S ribosomal subunit. *J. Med. Chem.* **51**, 3353–3356 (2008).
45. Polikanov, Y. S., Steitz, T. A. & Innis, C. A. A proton wire to couple aminoacyl-tRNA accommodation and peptide-bond formation on the ribosome. *Nat. Struct. Mol. Biol.* **21**, 787–793 (2014).
46. Huter, P. et al. Structural basis for polyproline-mediated ribosome stalling and rescue by the translation elongation factor EF-P. *Mol. Cell* **68**, 515–527.e6 (2017).
47. Thompson, J., O'Connor, M., Mills, J. A. & Dahlberg, A. E. The protein synthesis inhibitors, oxazolidinones and chloramphenicol, cause extensive translational inaccuracy in vivo. *J. Mol. Biol.* **322**, 273–279 (2002).

Methods

Generation of DNA templates for toeprinting analysis and smFRET experiments. DNA templates were generated by PCR reactions using AccuPrime DNA Polymerase (Thermo Fisher) and the appropriate 5-primer combinations of the oligonucleotides listed in Supplementary Table 1. For example, primers T7, NV1, SMFRET-Fwd, SMFRET-Rev and SMFRET-Mid(FKAFK) were used to generate the MFKAFK template. The structures of the resulting products are shown in Supplementary Fig. 1. In the PCR reactions, the T7 and NV1 primers were at 100 µM while the primers SMFRET-Fwd and SMFRET-Rev were at 10 µM. The template specific 'SMFRET-Mid' primers were at 10 µM.

Toeprinting assay. Toeprinting assays were conducted as previously described using the NV1 primer[48,49]. Briefly, translation reactions were performed in a total volume of 5 µl for 15 min at 37 °C by using PURExpress system (New England Biolabs). After subsequent addition of AMV reverse transcriptase (New England Biolabs), primer extension was carried out for 10 min. When indicated, CHL (Fisher Scientific), LZD (Pharmacia) and thiostrepton (Sigma Aldrich) were present in the reaction at a 50 µM concentration; in these cases, the inhibitors were pre-dried at the bottom of the reaction tubes before setting up the translation reactions.

Preparation of biotinylated RNA templates for smFRET in vitro translation assay. The smFRET DNA templates generated by PCR for the toeprinting experiments (see above) were ligated into SmaI-cut pUC18 vector and the resulting plasmids were transformed into *E. coli* JM109 cells (Promega). Following verification by Sanger sequencing of the constructs, plasmids were cut with EcoRI and used for in vitro run-off transcription with T7 RNA polymerase. Transcription reaction was carried out in the presence of Biotin-GMP to generate 5′ biotinylated RNA.

smFRET experiments. Detailed methods regarding purification of ribosomal subunits, translation factors, tRNA and specific reagent concentrations, buffer composition and incubation times have been previously described[30,32,33]. Briefly, synthetic fluorescently labeled DNA oligonucleotides were annealed to the 30S and 50S ribosomal subunits isolated from *E. coli* to obtain Cy3B-30S, BHQ-50S or Cy5–50S. Aminoacylated Cy3 or Cy5 labeled tRNAs were prepared as previously described, where purified tRNA (Chemical Block Ltd) was fluorescently labeled via NHS-chemistry (sulfo-cyanine3 or sulfo-cyanine5 NHS ester (Lumiprobe Co.), interacting with the acp^3U47 residue), high-performance liquid chromatography-purified and charged with amino acid using aminoacyl-synthetase.

Single-molecule experiments were carried out as previously described. Briefly, Cy3B-30S were mixed with protein S1 before incubation with biotinylated mRNA (prepared as described above), IF2 and $fMet\text{-}tRNA^{ini}$ to form pre-initiation complexes. In parallel, EF-Tu was charged with GTP by EF-Ts. Ternary complexes were formed by incubation of EF-Tu/GTP with both fluorescently labeled and bulk unlabeled tRNAs, where the bulk unlabeled tRNAs have been charged with a set of amino acids that lacks phenylalanine or lysine or both. Zero mode wavelength (ZMW) chips were prepared by pre-incubating the surface of the chip with Neutravidin (Thermo Scientific). Pre-initiation complexes containing biotinylated mRNA and Cy3B-30S were then immobilized onto the ZMW chip through Neutravidin-biotin interaction. Labeled 50S subunits (BHQ-50S or Cy5–50S, 65 nM), ternary complexes (50 nM), EF-G (50 nM), oxygen scavenging system (PCA and PCD purchased from Pacific Bioscience), triplet state quencher (TSY purchased from Pacific Bioscience) and, depending on the experiment, the inhibitors CHL and LZD (1–5 µM, as indicated), were mixed together and pipetted onto the ZMW chip containing pre-initiation complexes. Eight-minute videos at 10 frames per second of the translation reactions were recorded using PacBio RSII (Pacific Biosciences) while the fluorophores Cy3 (green) and Cy5 (red) were excited with 532- and 642-nm lasers, respectively.

Collected videos of fluorescence traces for each experiment were analyzed using the previously described pipe-line. Briefly, fluorescence traces that contained high Cy3B and Cy5 signals were selected using a custom script, and manually inspected for correlated Cy3B and Cy5 signals expected for translating molecules. Selecting criteria for intersubunit FRET experiments involved quenching of the Cy3B signal on 70S formation (due to Cy3B–BHQ FRET), followed by $Phe\text{-}(Cy5)\text{-}tRNA^{Phe}$ binding to the F_2 codon correlated to the nonrotated to rotated state transition. In the case of tRNA–tRNA FRET and the intersubunit FRET experiments using Cy3 (or Cy3B) and Cy5 pairs, selection criteria involved detecting an anticorrelated signal between Cy3 and Cy5 signals. States were assigned in the selected traces, which were used to calculate the number of observable elongation events, Cy5 pulse durations and the periods of nonrotated and rotated states. For nonrotated and rotated lifetime measurements or Cy5-pulse duration, times spent in each state across the entire population of molecules were collected and fitted with a single-exponential fit. For FRET efficiency measurements, a single Gaussian function was fitted to collected frames in each state. For calculation of the ribosome progression, the number of ribosomes translating a particular codon (showing both transitions to rotated and nonrotated state) were divided by the number of ribosomes translating the first elongation codons (F_2 or the second phenylalanine codon in all cases) and multiplied by 100 to calculate the percentage. Similarly, the drug efficiency was calculated as:

$$\text{Drug efficiency} = \frac{(n \text{ of ribosomes at codon 5} - n \text{ of ribosomes at codon 6})}{n \text{ of ribosomes at codon 5}}$$

and the error was estimated assuming the binomial distribution:

$$\text{Drug efficiency error} = \sqrt{\frac{\text{drug efficiency} \times (1 - \text{drug efficiency})}{n \text{ of ribosomes at codon 5}}}$$

For measuring tRNA–tRNA FRET efficiencies, experiments were carried out in the total internal reflectance (TIRF) microscope setup, for consistency with the previous reports. Briefly, pre-initiation complexes were prepared as outlined above, and mixed with the elongation factors (200 nM of EF-G and 6.7 µM of total tRNA ternary complex charged without Phe-AA and 500 nM of $Phe\text{-}(Cy3)\text{-}tRNA^{Phe}$) in the presence of 20 µM CHL, and incubated for 20 min in the room temperature, to form CHL-arrested elongation complexes. These were immobilized to the TIRF quartz slide that was functionalized with PEG/PEG-biotin before the experiment using biotin-Neutravidin interaction. Unbound complexes were washed out and the slide imaged in buffer containing PCA/PCD/TSY mix and 100 nM of $Lys\text{-}(Cy5)\text{-}tRNA^{Lys}$ for 5 min at 5 frames per second. The magnesium ion (Mg^{2+}) concentration has been adjusted to 15 mM total $MgCl_2$, to be consistent with the previous measurements.

Mischarging $Cy5\text{-}tRNA^{Lys}$ with glycine by the flexizyme reaction. $Gly\text{-}(Cy5)\text{-}tRNA^{Lys}$ was synthesized from flexizyme dFx-catalyzed reaction as previously described[41,42,50]. 3,5-dinitrobenzyl ester of glycine (Gly-DBE) was generously provided by H. Suga (University of Tokyo). The flexizyme (dFx) was prepared by run-off T7 transcription of the DNA template, followed by the FPLC-purification step. $tRNA^{Lys}$ (Chemical Block Ltd.) was labeled with Cy5 as described above. In the flexizyme reaction, final concentrations after mixing all the components were: a mixture of 100 mM HEPES-KOH pH 7.5, 10 µM dFx and 8 µM $Cy5\text{-}tRNA^{Lys}$, which was heated at 95 °C for 2 min and slowly cooled to room temperature over 5 min. Then $MgCl_2$ was added to the final concentration of 25 mM and the reaction was incubated at room temperature for another 5 min before cooling on ice for 3 min. Gly-DBE in DMSO was added to 5 mM from a 25 mM stock to initiate the charging reaction, which was incubated on ice for 5 h before quenching by the addition of final 300 mM NaOAc, pH 5.2. The charged tRNA was ethanol precipitated, resuspended in tRNA storage buffer (10 mM NaOAc pH 5.2 and 0.5 mM $Mg(OAc)_2$) and further purified by running through a P6 spin column equilibrated with the same tRNA storage buffer. Final tRNA was stored at −80 °C after flash freezing with liquid nitrogen, and was used for making the ternary complex as described above.

Statistics and reproducibility. Measurements from single-molecule fluorescence assay resulted from a specified number (n) of molecules from a single experiment.

Reporting Summary. Further information on research design is available in the Nature Research Reporting Summary linked to this article.

Data availability

All experimental data are available upon reasonable request.

Code availability

All MATLAB scripts used in this study are available upon request.

References

48. Vazquez-Laslop, N., Thum, C. & Mankin, A. S. Molecular mechanism of drug-dependent ribosome stalling. *Mol. Cell* **30**, 190–202 (2008).
49. Orelle, C. et al. Identifying the targets of aminoacyl-tRNA synthetase inhibitors by primer extension inhibition. *Nucleic Acids Res.* **41**, e144 (2013).
50. Wang, J., Kwiatkowski, M. & Forster, A. C. Kinetics of ribosome-catalyzed polymerization using artificial aminoacyl-tRNA substrates clarifies inefficiencies and improvements. *ACS Chem. Biol.* **10**, 2187–2192 (2015).

Acknowledgements

This work was supported by the US National Institutes of Health (grant nos. GM51266 to J.D.P. and R01 AI125518 to A.S.M. and N. V.-L.); by a Stanford Bio-X fellowship to J.C.; by the Knut and Alice Wallenberg Foundation postdoctoral scholarships to J.Z. and to J.W. (no. 2015.0406). We are grateful to H. Suga for providing the substrate for the flexizyme reaction and C. Innis for the advice and training in using the flexizyme-based procedures. We thank members of the Puglisi laboratory and the Mankin/Vázquez-Laslop laboratory for discussion and input.

Author contributions

J.C., J.M., N.V.-L., A.S.M. and J.D.P. conceived the project and designed the single-molecule experiments. J.M. performed the toeprinting assay. J.C. prepared the reagent,

and performed the single-molecule experiment and data analysis with the help of J.M. and J.W. J.Z. and D.-H.C. provided supporting data. J.C., J.M., J.Z., N.V.-L., A.S.M. and J.D.P. wrote the manuscript with the input of others.

Competing interests

The authors declare no competing interests.

Additional information

Supplementary information is available for this paper at https://doi.org/10.1038/s41589-019-0423-2.

Correspondence and requests for materials should be addressed to N.V.-L., A.S.M. or J.D.P.

Reprints and permissions information is available at www.nature.com/reprints.

nature chemical biology

SUPPLEMENTARY INFORMATION

https://doi.org/10.1038/s41589-019-0423-2

In the format provided by the authors and unedited.

Dynamics of the context-specific translation arrest by chloramphenicol and linezolid

Junhong Choi[1,2,4,6], James Marks[3,5,6], Jingji Zhang[1], Dong-Hua Chen[1], Jinfan Wang[1], Nora Vázquez-Laslop[3*], Alexander S. Mankin[3*] and Joseph D. Puglisi[1*]

[1]Department of Structural Biology, Stanford University School of Medicine, Stanford, CA, USA. [2]Department of Applied Physics, Stanford University, Stanford, CA, USA. [3]Center for Biomolecular Sciences, University of Illinois, Chicago, IL, USA. [4]Present address: Department of Genome Sciences, University of Washington, Seattle, WA, USA. [5]Present address: National Institute of Arthritis and Musculoskeletal and Skin Diseases, National Institutes of Health, Bethesda, MD, USA. [6]These authors contributed equally: Junhong Choi, James Marks. *e-mail: nvazquez@uic.edu; shura@uic.edu; puglisi@stanford.edu

Supplementary material for:
Dynamics of the context-specific translation arrest by chloramphenicol and linezolid

Junhong Choi[1,2,4,†], James Marks[3,5,†], Jingji Zhang[1], Dong-Hua Chen[1], Jinfan Wang[1], Nora Vázquez-Laslop[3,#], Alexander S. Mankin[3,#] & Joseph D. Puglisi[1,#]

Institutions

[1] Department of Structural Biology, Stanford University School of Medicine, Stanford, CA, USA

[2] Department of Applied Physics, Stanford University, Stanford, CA, USA

[3] Center for Biomolecular Sciences, University of Illinois, Chicago, IL, USA

Present addresses

[4] Department of Genome Sciences, University of Washington, WA, USA

[5] National Institute of Arthritis and Musculoskeletal and Skin Diseases, National Institutes of Health, Bethesda, MD, USA

[†] Authors contributed equally to this work

[#] Co-corresponding authorship (N.V.-L.: nvazquez@uic.edu, A.S.M.: shura@uic.edu, J.D.P.: puglisi@stanford.edu)

Supplementary Figure 1. Complete nucleotide sequences of DNA constructs used to generate mRNAs used in toe-printing and smFRET experiments. The sequences of the ORFs and the encoded proteins are shown in red, SD sequence is orange and T7 promoter is blue. Amino acids that distinguish the non-stalling templates (middle and bottom) from the stalling sequence (top) are boxed.

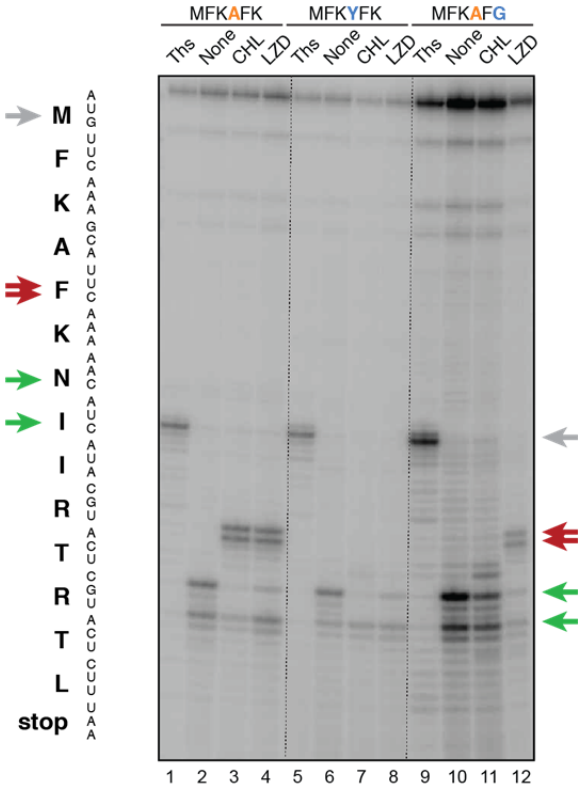

Supplementary Figure 2. Bypass of the CHL- or LZD-dependent arrest site during translation of the MFKYFK or MFKAFG templates. Translation of the mRNAs was carried out in the presence of thiostrepton, CHL or LZD. The toeprint bands corresponding to the ribosomes arrested at start codons by thiostrepton or at F_5 codons by CHL or LZD are shown by grey and red arrows, respectively. In addition, all reactions contained indolmycin, an inhibitor of Ile-tRNA synthetase causing translation arrest when the Ile codon enters the decoding center (green arrows). The absence of the 'F_5 codon' toeprint bands but the presence of the 'Ile-codon' bands in the CHL- and LZD- samples (the MFKYFK template) or CHL sample (MFKAFG template) indicates faithful translation past the arrest site. A portion of this gel is reproduced in the main **Fig 2c**. Similar results were independently observed at least two times.

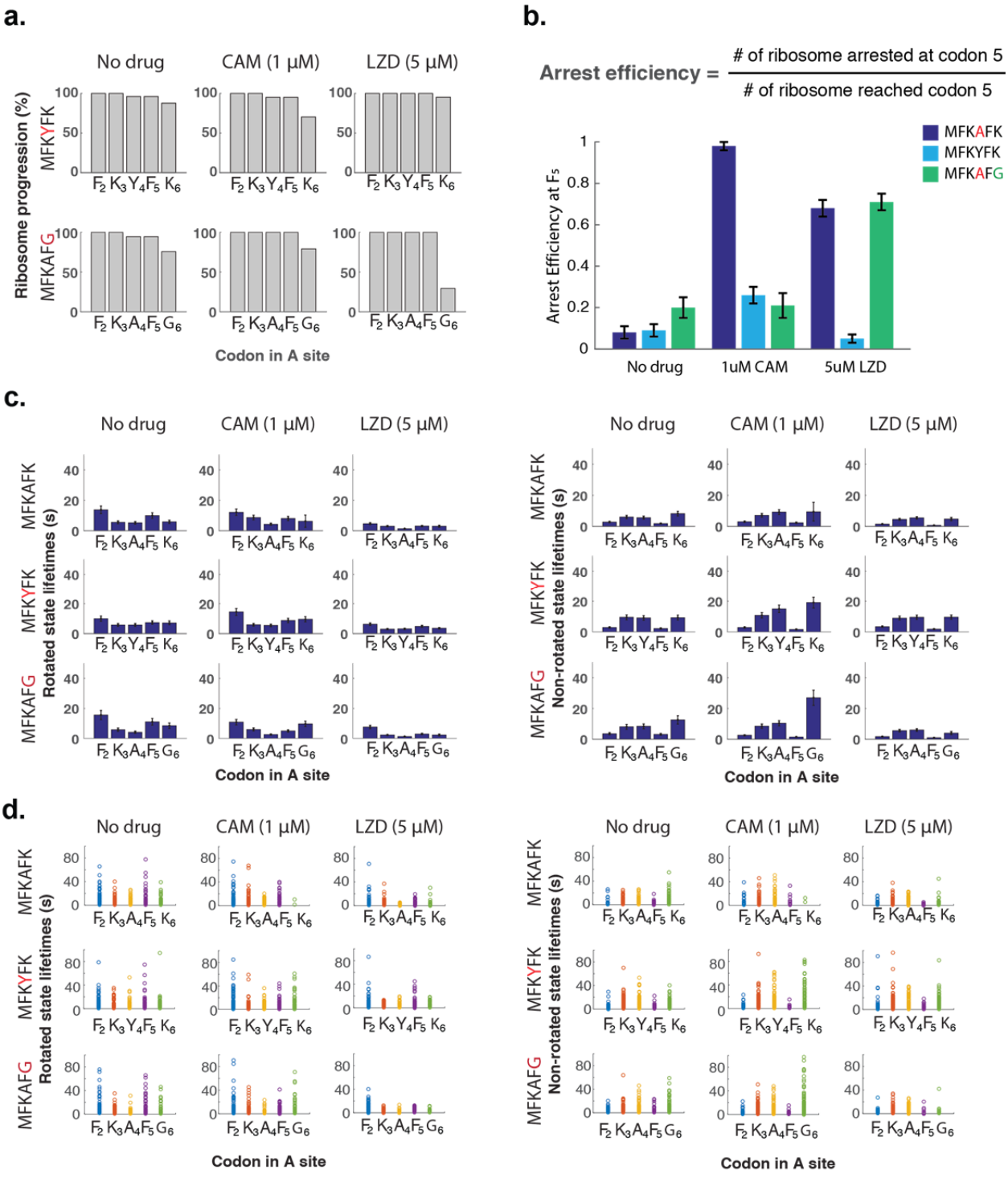

Supplementary Figure 3. Lifetime measurements and the arrest efficiency measurements for MFKAFK, MFKYFK and MFKAFG mRNA constructs using single-molecule FRET-based assay.

a. Processivity of translation measured for the first six codons at different conditions (n = 107, 121, 148, 74, 110 and 130 for plots from left to right and then from top to bottom). **b.** Arrest efficiency calculated for each condition in **a**. The error bar represents the s.e. from fitting the

binomial distribution to the difference in ribosome progression between codon 5 and 6. **c.** Rotated state (left) and non-rotated state (right) lifetimes measured for the first six codons translated at different conditions (n = 87, 100, 139, 107, 121, 148, 74, 110 and 130 for plots from left to right and then from top to bottom. Error bars represent 95% confidence interval from fitting the single-exponential distributions). **d.** Individual data points used to calculate the rotated (left) and non-rotated state (right) lifetimes shown in the panel **c**.

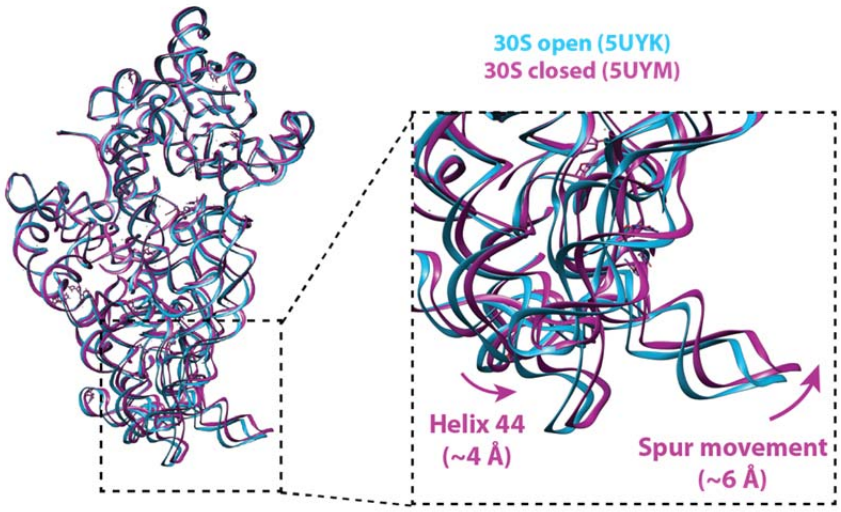

Supplementary Figure 4. Previously observed 30S domain closure moves the helix 44, where the Cy3B fluorescent probe is attached to the ribosome, towards the direction of the subunit rotation (structure adapted from PDB 5UYK and 5UYM from Loveland, A. B., Demo, G., Grigorieff, N. & Korostelev, A. A. Ensemble cryo-EM elucidates the mechanism of translation fidelity. *Nature* **546,** 113–117 (2017)).

PRIMER NAME	DNA SEQUENCE
T7 FX-F	GGCGTAATACGACTCACTATAG
FX-F	GTAATACGACTCACTATAGGATCGAAAGATTTCCGC
DFXR1	ACCTAACGCCATGTACCCTTTCGGGGAT GCGGAAATCTTTCGATCC
DFXR2	ACCTAACGCCATGTACCCT
MICROHELIX	GGCUCUGUUCGCAGAGCCGCCA
SMFRET-FWD	ATTAATACGACTCACTATAGGGCAACCTAAAACTTACACACG CCCCGGTAAGGAAATAAAAAT
SMFRET-MID(FKAFK)	GCCCCGGTAAGGAAATAAAAATGTTCAAAGCATTCAAAAACA TCATACGTACTCGTACTC
SMFRET-MID(FKYFK)	GCCCCGGTAAGGAAATAAAAATGTTCAAATACTTCAAAAACA TCATACGTACTCGTACTC
SMFRET-MID(FKAFG)	GCCCCGGTAAGGAAATAAAAATGTTCAAAGCATTCGGGAACA TCATACGTACTCGTACTC
SMFRET-REV	GGTTATAATGAATTTTGCTTATTAACCTTGCCTGCGCTTAAA GAGTACGAGTACGTATGATGT
T7	ATTAATACGACTCACTATAGGG
NV1	GGTTATAATGAATTTTGCTTATTAAC

Supplementary Table 1. DNA primers used to generate reagents for smFRET experiments